1960

Interferometric observations of the optical dispersion of carbon dioxide in the near infrared

Muncie, Wendell B.

Monterey, California: U.S. Naval Postgraduate School

INTERFEROMETRIC OBSERVATIONS OF THE OPTICAL DISPERSION OF CARBON DIOXIDE IN THE NEAR INFRARED

WENDELL B. MUNCIE
and
FREDERICK H. WITTEMORE

Mont 258

INTERFEROMETRIC OBSERVATIONS OF THE OPTICAL DISPERSION OF CARBON DIOXIDE IN THE NEAR INFRARED

* * * *

Wendell B. Muncie

and

Frederick H. Whittemore

INTERFEROMETRIC OBSERVATIONS OF THE OPTICAL DISPERSION OF CARBON DIOXIDE IN THE NEAR INFRARED

by

Wendell B. Muncie
Lieutenant Commander, United States Navy

and

Frederick H. Whittemore
Lieutenant, United States Navy

Submitted in partial fulfillment of
the requirements for the degree of

MASTER OF SCIENCE
IN
PHYSICS

United States Naval Postgraduate School
Monterey, California

1960

INTERFEROMETRIC OBSERVATIONS OF THE OPTICAL DISPERSION OF CARBON DIOXIDE IN THE NEAR INFRARED

by

Wendell B. Muncie

and

Frederick H. Whittemore

This work is accepted as fulfilling
the thesis requirements for the degree of
MASTER OF SCIENCE
IN
PHYSICS
from the
United States Naval Postgraduate School

ABSTRACT

This investigation was conducted at the U. S. Naval Postgraduate School, Monterey, California, by Lieutenant Commander Wendell B. Muncie, USN, and Lieutenant Frederick H. Whittemore, USN, during the period 1 August 1959 to 31 March 1960.

The investigation of the optical dispersion of gases in the near infrared region, particularly in the region of longer vavelengths, has become of increasing importance in recent years. Believing that a Rayleigh refractometer would result in more accurate measurements, an instrument of this type was used in the investigation.

The inherent weakness of low radiation intensity associated with a Rayleigh interferometer required modification of the basic instrument to a multi-channel tube in order to provide increased intensity necessary for observation to the limit of the near infrared range. Accordingly, optical components that would permit investigation between 1.8 and 24 microns were installed in the optical system. A vacuum and gas admission system capable of providing a pressure differential of one atmosphere, and incorporating fractional distillation for gas purification was used.

We wish to express our appreciation to Professor Sydney H. Kalmbach for his suggestion of this project, as well as for his assistance in pursuing it.

TABLE OF CONTENTS

LIST OF ILLUSTRATIONS

TABLE OF SYMBOLS

n	Index of Refraction
ω_{0i}	i^{th} Characteristic Frequency of Gas Molecule
ω	Frequency of Incident Electromagnetic Wave
N_i	No/Unit Volume of Oscillators of Characteristic Frequency and mass m_i
m_i	Mass of i^{th} Oscillator
A_i	Absorption Coefficient for i^{th} Characteristic Wavelength
λ	Wavelength of Incident Electromagnetic Wave
λ_i	i^{th} Characteristic Wavelength
m	Number of Fringes; or Integral Number
L	Geometrical Length of Interferometer
T	Temperature, ^{o}K
ΔP	Pressure Differential, Gas-Vacuum
I	Intensity
β	$\frac{1}{2}$ Phase Difference Across Slit of Width a, $\beta = \frac{\pi a \sin\theta}{\lambda}$
γ	$\frac{1}{2}$ Phase Angle of Adjacent Slits, $\gamma = \frac{\pi d \sin\theta}{\lambda}$
N	Number of Slits
a	Slit Width
d	Slit Distance, Distance between Centers of Adjacent Slits
θ	Angle between the Plane of the Slit and the Normal to the Incident Radiation
s	Detector Slit Width
f	Focal Length of Paraboloidal Mirror
$\delta\theta$	Angular Halfwidth of Principal Maxima
W	Distance, Edge of Mask Slit to Side of Channel
D	Width of Channel
g	Exit Slit Width

R	Resultant Amplitude of Six Slits
R_1	Resultant Amplitude of One Set of Alternate Slits
R_2	Resultant Amplitude of Second Set of Alternate Slits
R_o	Amplitude Contribution of One Slit
ϕ	Phase Difference

1. INTRODUCTION.

The investigation of optical dispersion of gases by interferometric means has long been a subject of interest, with the majority of the investigations being conducted in the visible region of the spectrum. In recent years interest has shifted primarily to the infrared region, and considerable investigation has been conducted in the shorter near-infrared band, but with gas prisms rather than the Rayleigh interferometer.

With the belief that the Rayleigh refractometer (or interferometer) would produce more accurate results, investigation in the visible and near infrared region has been conducted at the U. S. Naval Postgraduate School since 1956 with this instrument. The inherent weakness of radiation intensity, however, limited investigation to 3 microns. In order to extend the region of investigation to the limit of the near infrared (25 microns), Eaton and Thomas [1] designed and constructed a six-channel Rayleigh tube, and associated dual manifold vacuum and gas admission system, in order to increase the radiation detection capabilities by a factor of nine.

Our investigation was conducted with the Eaton-Thomas apparatus, modified slightly to improve gas purification and ease of optical alignment. A detailed description of the equipment may be found in Sections 6 through 10.

Wetterblad and Statescu [10] had previously investigated carbon dioxide to 13.75 microns. With the Eaton-Thomas tube we were able to extend this range to 24 microns. Both Wetterblad's and Statescu's results are tabulated in Section 15 (Table 1) and plotted (Figures 14 and 15) for comparison.

2. THEORY OF DISPERSION IN GASES.

Gaseous molecules, containing positive and negative charges, can be considered as an assemblage of oscillating dipoles which emit electromagnetic radiation of one or more frequencies characterized by the oscillatory mode(s) of the atoms. Any molecule containing N atoms has 3N kinds of motion. Three modes are translational, three are rotational (two if a linear molecule) about the axes of inertia, and the remainder are vibrational (vibration-rotation). The vibrational modes are those responsible for producing the phenomena of absorption in the near infrared region. Each of these 3N-6 (3N-5 if the molecule is linear) modes of vibration has its own characteristic vibrational frequency. [2].

When electromagnetic radiation is passed through a gaseous medium, the varying electric field of the incident waves impresses forced vibrations on the gas molecules. The resultant oscillations of the molecules can be considered as the result of an elastic restoring force (which is responsible for the free oscillations of the molecule), an external sinusoidal force (imposed by the electric field), and a frictional force (responsible for damping).

In gases the dissipative forces are small except when the frequency of the electromagnetic wave is in the neighborhood of a characteristic frequency of the molecule, in which case the amplitude of the forced oscillations becomes large and the gaseous medium exhibits strong absorption. This phenomenon is referred to as resonance absorption, similar to the phenomenon of acoustic resonance, demonstrated by the forced oscillations of a tuning fork by a sound wave of frequency equal to the characteristic frequency of the fork. [3].

In the neighborhood of a characteristic frequency the index of refraction of the absorbing medium exhibits "anomalous" behavior. As

the frequency of the radiation approaches that of the characteristic frequency of vibration (from a lesser value) the index of refraction decreases instead of increasing, known as anomalous dispersion. As the two frequencies near each other the index of refraction reaches a maxium, reverses abruptly, reaches a minimum when the frequency of the electromagnetic radiation is slightly higher than the characteristic frequency of the absorping medium, and then exhibits normal behavior. [3] . This phenomenon is explained by the frequency dependence of the index of refraction, from the following equation:

$$n^2 = 1 + \frac{\epsilon^2}{\epsilon_0^2} \sum_i \frac{N_i/m_i}{\omega_{oi}^2 - \omega_o^2}$$

Were it not for damping forces, a mathematical discontinuity would occur when $\omega = \omega_o$. This condition is approached for gases, whose absorption lines are very narrow. The behavior of the index of refraction and the absorption coefficient near resonance is shown in Figure 1.

Sellmeier deduced a formula which is practically identical to the electromagnetic dispersion formula, and which represents dispersion for those wavelengths for which the medium is comparatively transparent, i.e. on both sides of the absorption band(s):

$$n^2 = 1 + \sum_i \frac{A_i \lambda^2}{\lambda^2 - \lambda_i^2}$$

In the case of very long wave lengths the λ_i term can be neglected and we have $n = \sqrt{1+\Sigma A_i}$. [5] . Since $\sum_i A_i$ is small for a gas, the index of refraction approaches $1 + \frac{\Sigma A_i}{2}$.

For the interested reader a detailed treatment of molecular structure may be found in Harrison, Lord, and Loofbourow [2] , and an excellent development on the theory of gaseous dispersion may be found in Rossi. [3] .

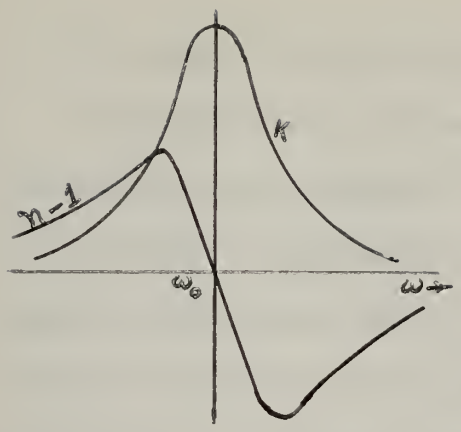

Figure 1. Anomalous dispersion, showing index of refraction and absorption coefficient as functions of frequency.

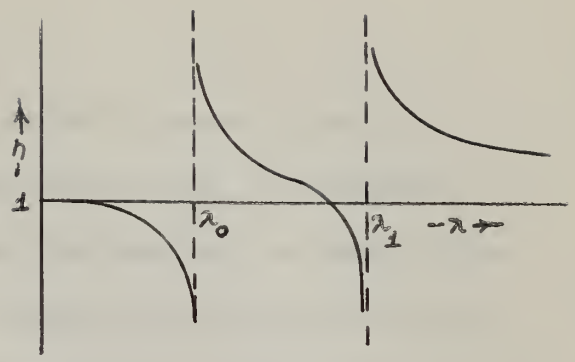

Figure 2. Theoretical dispersion curves given by Sellmeier's equation for a medium having two natural frequencies.

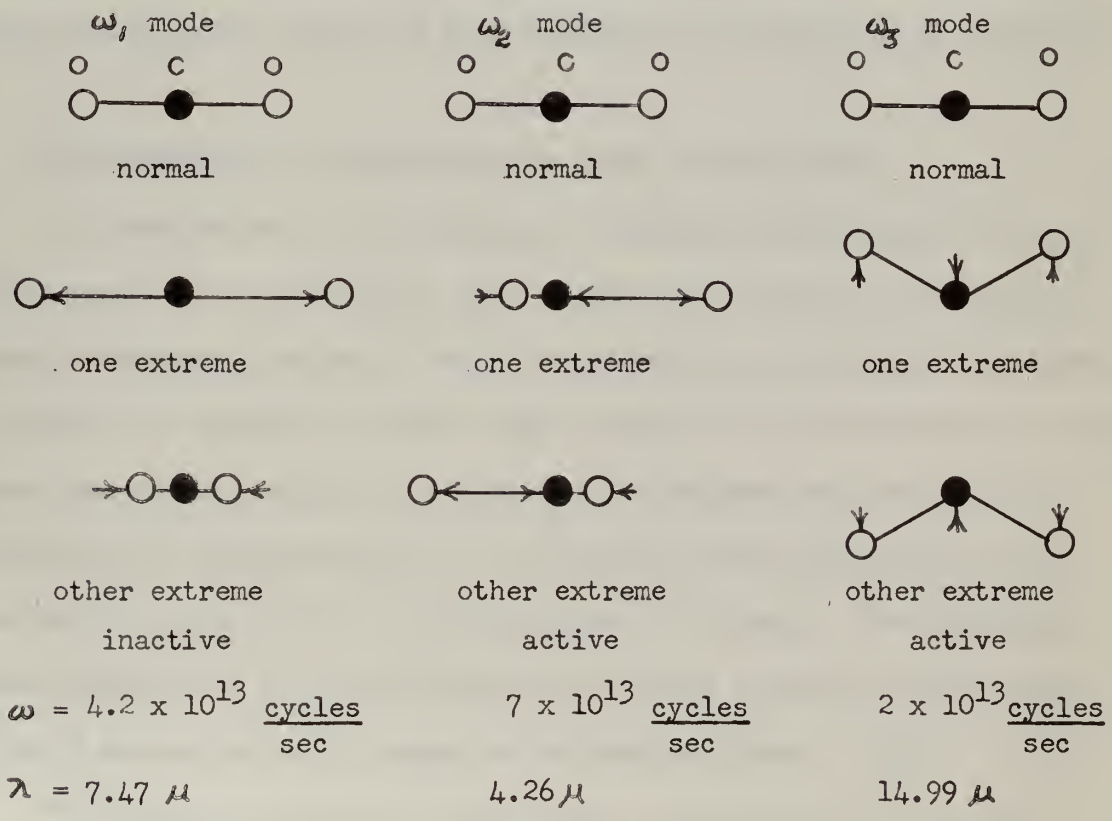

Figure 3. Vibrational modes of the carbon dioxide molecule with accompanying frequencies and wave lengths. ω_1 mode is inactive.

3. THE CARBON DIOXIDE MOLECULE.

The carbon dioxide molecule is a linear triatomic molecule exhibiting central symmetry. There are 3N-5=4 modes of vibration, and therefore 4 fundamental vibrational frequencies. One mode is degenerate and another (see ω_4 mode in Figure 3) is not active in the infrared since it does not produce a change in the dipole moment. It is observed in the Raman spectrum, however, as there is a change in polarizability associated with this infrared-inactive vibrational mode.

In the near infrared range carbon dioxide exhibits absorption at 1.40, 1.60, 2.06, 2.77, 4.26, 4.82, 5.17 and 14.99 microns. The most significant regions are those centered about 4.26 and 14.99 microns, these bands being associated with fundamental frequencies of vibration.

4. INTERFEROMETRIC DETERMINATION OF INDEX OF REFRACTION.

An interferometer, by dividing a collimated monochromatic beam of light into two or more parts, then rejoining the beam to form interference fringes, provides a means for measuring the refractive indices of gases. By passing the split beam through two different media of the same geometrical length, it is possible to measure the optical path difference by interpretation of the observed fringe pattern and its variation as the optical path difference is altered. "The Rayleigh Refractormeter is by far the most accurate and convenient means available of measuring small changes of refractive index." [7] .

The modified Rayleigh refractometer, constructed by Eaton and Thomas, was designed to measure the index of refraction of a gas with respect to a vacuum. This is accomplished by passing one half of the incident beam through alternate evacuated chambers, while the other

half of the beam is passed through chambers to which gas is admitted at a controlled rate. The change in density of the gas as the pressure is increased lengthens the optical path in the gas, and the position of the fringe pattern shifts. To an observer this pattern shift appears as alternate maxima and minima traveling laterally across a detector slit, the width of which is adjusted to permit no part of more than one maximum (or minimum) to be observed.

The basic equation for determining variation in the indices of refraction of two media is:

$$n_2 - n_1 = \frac{m\lambda}{L}$$

This reduces to $n - 1 = \frac{m\lambda}{L} \frac{T}{273.16} \frac{760}{\Delta P}$ for a correction of the index of refraction of the gas to 0°C and 760 mm pressure, using a vacuum as the standard medium. [8] . This, of course, is the equation for an ideal gas and must be further corrected for deviation from the ideal gas law. The Beattie-Bridgeman equation of state is the most accurate of all for carbon dioxide [9] , and, together with a density correction for mercury, was used in reducing our data.

5. THE ADVANTAGE OF A MULTIPLE CHANNEL INTERFEROMETER.

Low radiation intensity is the major difficulty encountered in using the Rayleigh Interferometer. This drawback can be overcome by increasing the intensity of the radiation source or by modifying the instrument. Our source was the Perkin-Elmer Model 13 Infrared Spectrophotometer, which, when operated at peak power still produced insufficient radiation intensity for fringe detection at the long wavelength end of the infrared spectrum. The alternative, then, was to modify the instrument to increase the intensity of interference maxima.

The following equation shows the effect on the principal maximum of a Fraunhofer diffraction pattern of N equally spaced slits of equal aperture:

$$I = I_o \frac{\sin^2 \beta}{\beta^2} \frac{\sin^2 N\gamma}{\sin^2 \gamma}$$

For small values of the phase angle γ, $I \sim N^2$. From this premise came the idea, and subsequent design and fabrication by Eaton and Thomas, of an interferometer which would result in an increase in intensity by increasing the number of channels.

In order to maintain the proper phase relationship between radiation travelling separate channels in the gas and vacuum, and have it recombine to form proper maxima and minima, it was necessary to design the tube so that alternate chambers were evacuated, the remaining chambers being opened to controlled admission of the gas. Appendix III deals with the mathematical development of the phase relationships of radiation from alternate slits.

The instrument, optical system and gas-vacuum system are excellently described by Eaton and Thomas [1]. Their design and construction procedures are described in the following sections, with slight modification in the dual manifold, gas-vacuum system, detector slit, and optical alignment procedures.

6. GENERAL DESCRIPTION OF INSTRUMENTATION.

The system illustrated in Figures 10 through 13, and as designed specifically for the interferometric analysis of the indices of refraction of gases, consists of the following components:

a. A Perkin-Elmer Infrared Spectrophotometer, Model 13, with NaCl and KBr prisms, utilized as (1) the source of infrared energy and (2) the

means of selection of monochromatic wave lengths in the region of the spectrum being investigated.

b. A modified version of the Rayleigh Refractometer, utilizing six energy transmitting channels instead of two. A more detailed description follows in Section 7.

c. A vacuum system capable of sustaining a vacuum of one micron of Hg for a period greater than four minutes with the fore-pump turned off, and with the provision for evacuating alternate channels as desired.

d. A gas system closely allied with the vacuum system which permits admission of the gas under investigation into the channels of the refractometer, alternate to those evacuated.

e. An optical system for directing the infrared energy from the monochromator through the refractometer to the energy detector.

f. A pressure differential measuring system consisting of a mercury manometer gauge capable of registering a pressure differential of slightly greater than one atmosphere, and a cathetometer equipped with a vernier permitting readings directly to 0.05 mm.

g. A chromel-alumel thermocouple and associated potentiometer for determining the temperature of the refractometer.

h. A PbS detector for the range 1.0 to 2.9 microns; and a thermocouple detector containing a KBr window, highly transparent to infrared radiation, for use in the 2.9 to 25 micron range.

i. A Leeds and Northrup Speedomax Recorder, Type G, for the continuous graphical presentation of energy received by the detector.

7. MODIFIED RAYLEIGH INTERFEROMETER.

In the matter of terminology, the modified Rayleigh Interfero-

meter will be referred to interchangeably as a refractometer, interferometer, or tube.

The interferometer has basic dimensions as follows:

Length	49.520 cm	
Width	5.897 cm	outside
	3.377 cm	inside
Height	5.940 cm	outside
	3.427 cm	inside
Channel width	0.478 cm	
Partition width	0.102 cm	

This interferometer is the heart of the system, and was designed and fabricated for the purpose of investigation of any gas in the entire near-infrared region. A description of the theory of operation of this instrument is contained in Section 4.

The sides, top and bottom of the instrument are basically one-half inch thick brass plates, cut to size, milled with slots for the five channel partitions and dovetailed at the corners to provide a smooth, tight fit. The partitions are of thin brass sheet 1.02 mm thick extending the full length of the tube. The dovetail joints and the partitions were silver soldered together with 430 solder to give as tight a seal as possible. After soldering, the ends of the tube were machined parallel and polished smooth.

On the top plate, two groups of three slots were cut completely through the brass. Each group opens to alternate channels. Over the top of each group of slots a brass manifold, topped by a vacuum coupling connector for receiving a glass tube, was secured by screws

and made vacuum tight by a neoprene gasket.

Five coats of Glyptal enamel were baked on the interior and two coats on the exterior of the tube.

At either end, flanges were attached by screws. These flanges serve the purpose of securing spring-loaded discs which hold the special windows that seal each end of the tube. The end windows mounted for this investigation are of KBr, 6 mm thick and 55 mm in diameter. The size of these windows was the limiting factor in determining the size, and therefore, the number of chambers in the interferometer. The KBr windows were sealed against the end of the tube with thin latex rubber gaskets, lightly coated with silicon vacuum grease, providing a vacuum seal around the circumference of the windows and along the partitions. A word of caution in using heat near the windows is in order, since KBr crystals are extremely susceptible to cracking from direct heat. They are also susceptable to clouding if the relative humidity is greater than 40%.

A thin metal mask with slits 3.85 mm wide and 5.80 mm between slit centers was fitted over one end to provide the proper interference pattern. (See Appendix II for slit width determination.)

When mounted for operation the tube is held in special mountings permitting vertical and lateral adjustment.

8. VACUUM AND GAS ADMISSION SYSTEM.

This system was designed with simplicity and flexibility foremost in mind. It is an integrated system in which vacuum or pressure can be applied as desired to either manifold of the interferometer. The entire system is illustrated schematically in Figure 11 and

photographically in Figures 12 and 13. The glass tubing is 12 mm diameter pyrex. All auxiliary apparatus such as stopcocks, stoppers and traps are of high vacuum design and also made of pyrex glass. Flexible rubber vacuum hose was utilized in connections to the interferometer and to the vacuum pump. The pump, a Duo-Seal Vacuum Pump, maintains a vacuum slightly below one micron. One trap cooled by liquid air was placed in the system just ahead of the vacuum pump to rid the system of contaminants and to collect used gas after completion of experimental runs. Near this same position a stopcock is installed for either venting the system or for providing a vacuum take-off to a Pirani gauge. By proper positioning of the stopcocks, vacuum can be maintained on either side of the mercury manometer and associated manifold of the interferometer.

The gas to be investigated can be admitted to the system under slight pressure and allowed to flow immediately to liquid air trap #1 (See Figure 11), where it can be purified by fractional distillation. It is then trapped in the #2 liquid air trap for use in the system. By careful manipulation of the liquid air container it can be admitted to the system at a controlled rate. The proper placement of stopcocks permits the gas to flow to either side of the manometer tube and interferometer, the other side remaining evacuated.

In our case we used four fractional distillations for purification. First, a large bottle of carbon dioxide (of purity known to be greater than 99.5%) was frozen in liquid air. With the gas, water vapor, and contaminants of melting points higher than the temperature of liquid air still frozen, gaseous contaminants were pumped off. The liquid air was then removed from the large container, and several

atmospheres of carbon dioxide were trapped in an evacuated lecture bottle, while the contaminants were still frozen in the larger container. The lecture bottle was used as our source for the entire investigation, and was re-frozen prior to admission to our system. Between runs the entire system was kept evacuated, all stopcocks open to the pump except #1. Prior to gas admission stopcocks 4 through 7 were closed, the gas bottle connected with vacuum hose to stopcock #1, which was then opened to evacuate the gas admission system up to the venting valve on the gas bottle. Liquid air was removed from the gas bottle and placed under trap #1, the valve on the gas bottle opened, and a sufficient quantity of gas trapped for several days runs. #1 stopcock was then closed and the bottle removed.

When we were ready to make experimental runs, the Dewar flask on #1 trap was lowered, and sufficient gas was trapped for a full day's observations in trap #2.

One side of the tube had twice the leak rate of the other (700 microns in three days, from the end windows), and was therefore used as the vacuum side. Since the forepump and associated liquid air trap could keep this side at a vacuum of less than 1 micron, the better side of the tube, leakwise, was used for gas admission, insuring that any contamination of the purified gas was negligible.

When ready to commence runs, stopcocks 2, 3, 5, and 6 were closed, 4 opened to the gas supply, and 7 opened to the forepump. Gas entry was carefully controlled by lowering the Dewar flask on trap #2. At the end of the run stopcock #4 was closed and the Dewar

flask raised. The pressure variation and temperature were then noted on the speedomax chart recording of the fringe count; after which the gas was re-trapped, stopcock #6 opened to the vacuum system until the pressure was less than 1 micron, and then closed in preparation for the next run. With this procedure as many as 45 runs have been made in a 12 hour period. For accurate partial last fringe count it is necessary to slow the gas admission at the last part of the run. However, any run requiring more than fifteen minutes was considered wasteful of time and poor operator procedure, except when investigation was being conducted in regions of extremely low intensity (near absorption bands and near the limits of the prisms). Here, a run could take as long as 30 minutes.

At the end of the day's runs, the carbon dioxide in trap #2 was permitted to escape to the contaminant trap, and all stopcocks except #1 were opened to the vacuum system. This permitted the system to remain evacuated at less than 1 micron, and would allow the gas to be pumped off should the liquid air on trap #1 evaporate to the point where some of the frozen gas sublimated. An unfortunate accident of this nature happened to us in December, blowing up the system and spreading mercury throughout the glass tubing and interferometer. This resulted in considerable loss of time while an entire new vacuum system was constructed. Stopcocks 1 and 3 were added at this time to aid in gas purification.

9. OPTICAL SYSTEM.

As shown in Figures 9, 10, and 12, the optical system consists of (1) source slit, which is actually the exit slit of the monochro-

mator; (2) a 14° off-axis paraboloidal mirror for directing parallel rays of energy through the interferometer, via a plane mirror necessary for reversing direction; (3) the interferometer; (4) a second 14° off-axis paraboloidal mirror for focusing the interference pattern at the detector slit; (5) the detector slit, set in width for receiving one interference fringe at a time (See Appendix I for mathematical discussion of slit width determination); (6) an ellipsoidal mirror for focusing the detector slit energy on the detector; and (7) a PbS detector, or thermocouple with matched preamplifier. Here again design centered around the need for simplicity, flexibility, accessibility, and ease of alignment.

Two 120 cm optical benches equipped with traversing supports are used to support the optical system. The first paraboloidal mirror is mounted facing the exit slit of the monochromator. Since this results in the wrong direction for the flow of energy, a plane mirror was placed so as to reverse the energy toward the interferometer, which is mounted on one of the optical benches. The details of the interferometer have previously been discussed in Section 7, and it need only be mentioned here as being a portion of the optical system.

For adjustment purposes, a specially designed support plate of 3/16" aluminum was mounted on three traversing supports, two on one optical bench and the third on the other bench. The main purpose of this plate is to permit accurate alignment of the detector, ellipsoidal mirror, detector slit, and the second 14° paraboloidal mirror. By traversing the support plate and pivoting the paraboloidal mirror, it is possible to align the detector with the interferometer. The basic layout of the optical system permitted the removal of one mirror

which had been required in previous layouts, and reduced the optical path to approximately 210 cm from exit slit to detector.

Provisions were made for mounting a prism and long focus microscope adjacent to the detector slit so that optical alignment in the visible range can be established or checked. Normally the green line of mercury is utilized, passed through our system by setting the wave length drum of the monochromator at 19.860.

10. RECORDING COMPONENTS.

A Leeds and Northrup Speedomax, Type G recorder was utilized while taking data. This recorder receives its signal from the amplifier associated with the Model 13 Spectrophotometer. The amplifier input is provided by the preamplifier of the thermocouple detector or by the PbS detector. Intensity of a fringe is amplified to cause pen deflection, and the amount of pen deflection is controlled by the response, gain, and full-scale controls on the control panel.

A mercury manometer capable of indicating a pressure differential of one atmosphere was installed with one arm attached to each manifold of the interferometer. Considerable care was taken in the construction and mounting of the manometer to insure an optically clear tube in the region where measurements of the menisci would be taken, and to provide a strong support to prevent accidental breakage. A cathetometer was mounted at the end of the optical benches (approximately 6 feet from the manometer) in such a position as to bring the sighting telescope in a line perpendicular to the plane of the vertically mounted manometer. Sighting of the menisci are facilitated by placing a light background behind the tube. Direct readings with an

accuracy of 0.05 mm are obtainable from the vernier of the cathetometer.

Measurement of the temperature of the interferometer is accomplished by a chromel-alumel thermocouple, using a Rubicon Precision Potentiometer for measuring potential difference, with a standard reference at 0°C. Conversion of the potential difference to temperature is made by use of standard tables.

11. SYSTEM CHECKS AND OPTICAL ALIGNMENT.

The initial system check of the Model 13 Spectrophotometer was conducted in August 1959 [11] and resulted in the replacement of several component parts, including a regohm regulator and the Nernst glower; and the complete adjustment of the slits and slit drive mechanism of the monochromator. Several runs with the spectrophotometer in double beam operation were made in order to check the infrared absroption of ammonia and polystyrene plastic film. These results compared closely to those found in the literature [11] , indicating satisfactory operation of the instrument. For the investigation of gases the spectrophotometer was returned to single beam operation.

The alignment of the exterior optical system was accomplished with considerable difficulty. The first paraboloidal mirror required remounting in order to place its center at the exact height of the middle of the exit slit. The mounting plate was attached to the monochromator, having been machined to permit lateral and longitudinal adjustment of the paraboloidal mirror. The mirror was bolted rigidly in place at the approximate focal length from the exit slit, rotated

approximately 7° off-axis laterally, and the vertical axis exactly aligned. The final adjustment was made with the longitudinal and lateral adjusting screws on the mirror, so as to obtain the sharpest possible image of the exit slit in the field of a collimated telescope, set 14° off axis.

The heights of the levelled monochromator and interferometer had previously been adjusted so that the center of the exit slit and longitudinal axis of the tube lay in the same horizontal plane. Therefore, the plane mirror, at the same level, required adjustment around the vertical and lateral axes only in order to pass parallel light through the tube. When aligned properly, the image of the exit slit appeared in the exact center of each channel of the interferometer, as viewed from the end farthest from the monochromator, and clear images of the mask slits could be seen on a piece of white paper held in the path of the light.

The 3/16" plate was then adjusted so that a line through the ellipsoidal mirror, detector, and detector slit intersected the longitudinal axis of the interferometer in the center of the second off-axis paraboloidal mirror at an angle of 14°, the heights of all four having been previously adjusted so that their centers lay in the same plane as the rest of the optical system.

The detector slit had been fixed longitudinally at the long focal point of the ellipsoidal mirror, the detector at the short focal point, and the paraboloidal mirror at its focal distance from the detector slit, all adjustments approximate.

The final adjustments were made as follows:

a. Lateral and vertical adjustment of the paraboloidal mirror

until the pattern of the mask centered on the detector.

b. Longitudinal adjustment of the paraboloidal mirror until the fringes were located in the plane of the detector slit.

c. Lateral adjustment of the detector slit until the principal maximum lay in the exact center of the slit (assuring that each fringe count from a completely evacuated tube commenced at the height of a maximum).

d. Longitudinal, lateral, and vertical adjustment of the ellipsoidal mirror to obtain the greatest signal indication on the recorder. This adjustment was the most critical of all in the regions of low signal intensity, 1/64" error in longitudinal adjustment being sufficient to cut the recorded fringe amplitude by a factor of one-half.

Optical alignment, with the exception of the final step was achieved with a mercury arc lamp, focused on the monochromator entrance slit through a 45-45-90 prism attached to a metal plate that fits in the plate guides on the side of the monochromator. The final step required use of the Nernst Glower as the energy source.

From day-to-day the second paraboloidal mirror adjustment should be checked, and, without fail the ellipsoidal mirror adjustment should be checked prior to commencing runs. We found it necessary to realign the ellipsoidal mirror as many as three times in one day.

12. WAVE DRUM CALIBRATION.

The calibration of the NaCl prism was accomplished with little difficulty, by using the absorption spectra of a thin Polystyrene plastic film, atmospheric H_2O and CO_2, and NH_3 (vapor from a bottle of NH_4OH drawn into an evacuated 10 cm gas cell). All the points publish-

ed in the Perkin-Elmer instruction manual [11] ; and by Downie, Magoon, Purcell, and Crawford [12] ; were located, and plotted on a calibration curve measuring 2 feet by 3 feet. All the points plotted on a smooth curve, and there was no doubt about ability to read the chart accurately to 0.01 μ wave length. The data published by Downie, et al, was most helpful; we used the same procedures (constant, rather than programmed slits). However, all of our calibration data was taken with single-pass beam, with the wave drum speed control set at four minutes per revolution. Also, each of the published spectra was broken into portions, with the gain and slit width re-set so that commencement of each portion had maximum amplitude on the recorder, insuring positive indentification and precise reading of the absorption points. Our calibration curve, on a reduced scale, is plotted in Figure 14. Note that the Hg green line is set at wave drum number 19.860, rather than 20.000, however.

The KBr prism required a little more effort to calibrate, since there was no rough comparison spectrum provided by Perkin and Elmer for this prism. The Littrow mirror was adjusted until the green Hg line lay at 21.000 on the wave drum. The NH_3 and atmospheric CO_2 spectra were run for rough check points, wave length versus wave drum, and then re-run for positive identification. The rather drastic methods used by Downie, et al, were avoided in attaining methanol vapor for the remainder of the calibration curve. We found that filling an evacuated 10 cm cell from the vapor above the surface of a beaker of methanol that had been heated in boiling water provided adequate concentration for absorption. All the published points were located and plotted on a chart of the same dimensions as that used for the NaCl prism. Here, also, the

chart was accurately readable to 0.01 μ.

To double check the KBr wave drum calibration, the fringe counts previously determined on the NaCl prism were re-run on the KBr prism in the overlap range at 11.58 and 13.44 μ. They checked exactly. Our calibration curve, on a reduced scale, is plotted in Figure 15.

13. EXPERIMENTAL RUN TECHNIQUES.

The following procedures were used in making an experimental run:

a. The wave drum was set for the desired wave length, by manually dialing in the wave drum number, always from a setting higher than the one desired (in the same direction that the wave drum was run for calibration).

b. The exit slit was set to approximately 20 λ (maximum of 30λ was used near absorption bands).

c. The detector slit was set between 15 λ and 20 λ, depending upon exit slit opening. The slit used had double-action jaws, and was calibrated from 0 to 500 μ. Therefore, it was not necessary to remove the slit or reset it laterally for different wavelengths. Since the jaws opened equally, it was a simple matter of rotating the thumb screw to the setting previously determined by the calibration.

d. The recorder controls were set as necessary to give clearly readable fringes. In some regions the signal return was sufficient to give full pen swing with the "gain" control set at 12 and "full scale" at 6. The minimum pen swing was 3/4" with full "gain", maximum "full scale", and "response" set at 3. The wave length selected determined the recorder control settings. The current was controlled manually, and a maximum of 0.86 amperes was used.

e. Admission of the gas has previously been discussed. However, in regions near an absorption band, a preliminary run was made to determine the pressure differential at which the fringes washed out. The recorded runs were then stopped short at a pressure where the fringe count could accurately be determined. In regions where the energy was not absorbed, the experimental runs were made to a pressure differential of approximately one atmosphere.

14. ESTIMATED ERROR.

An estimate of the maximum error in the value of the observed index of refraction can be made by considering the individual effects in measurement of all the quantities used to calculate the index of refraction. Differentiation of the equation, $n-1 = \left(\frac{760}{273.16}\right)\left(\frac{m\lambda T}{L\Delta P}\right)$ leads to: $\frac{dn}{n-1} = \frac{dm}{m} + \frac{d\lambda}{\lambda} + \frac{dT}{T} - \frac{dL}{L} - \frac{d(\Delta P)}{\Delta P}$

The maximum error would occur from the summation of the absolute values of the individual measurements:

a. Fringe count for individual runs, where the observed number of fringes was readable to 1/20th of a fringe at long wave lengths (few fringes) or near an absorption band at a frequency less than that of the characteristic frequency (few fringes). The maximum probable error occurred at 14.00 microns, where $\frac{dm}{m} = \frac{0.05}{4.3} = 1.16\%$

In the region of greater interest the maximum probable error occurred at 24 microns where $\frac{dm}{m} = \frac{0.05}{9.3} = 0.54\%$

The least probable error occurred where the fringe count was greatest, and where the number of fringes was recorded to the tenth of one fringe. At 1.825 microns $\frac{dm}{m} = \frac{0.1}{141.7} = 0.071\%$

The average fringe count for the entire range was 27.2 fringes, and $\frac{dm}{m} = \frac{0.1}{27.2} = 0.37\%$

b. Wavelength, where the maximum probable error occurred at the shortest wave length, and

$$\frac{d\lambda}{\lambda} = \frac{0.01}{1.825} = 0.548\%$$

c. Temperature, readable to 0.1°, and

$$\frac{dT}{T} = \frac{0.1}{297} = 0.03\%$$

d. Length of interferometer, where measurement was accurate to 0.001 inch, and $\frac{dL}{L} = \frac{0.001 \times 2.54}{49.520} = 0.005\%$

e. Pressure measurement, where the minimum pressure differential was recorded at 4.40 microns wavelength, and

$$\frac{d(\Delta P)}{\Delta P} = \frac{0.05}{103.65} = 0.048\%$$

Therefore, the maximum probable error for an individual run at the points representing (1) shortest wavelength, (2) intermediate unabsorbed wavelength less than 15 microns, (3) near an absorption band, (4) intermediate unabsorbed wavelength greater than 15 microns, and (5) longest wavelength, would be:

	λ	:	$\frac{\lvert dm \rvert}{m}$ +	$\frac{\lvert d\lambda \rvert}{\lambda}$ +	$\frac{\lvert dT \rvert}{T}$ +	$\frac{\lvert dL \rvert}{L}$ +	$\frac{\lvert d(\Delta P) \rvert}{\Delta P}$ =	TOTAL ERROR
(1)	1.825	:	0.071	0.548	0.03	0.005	0.007	0.66%
(2)	10.00	:	0.53	0.10	0.03	0.005	0.007	0.69%
(3)	14.00	:	1.16	0.07	0.03	0.005	0.014	1.28%
(4)	20.00	:	0.42	0.05	0.03	0.005	0.007	0.51%
(5)	24.00	:	0.54	0.004	0.03	0.005	0.007	0.63%

Obviously, in wavelengths greater than 3.0 microns the significant portion of the maximum probable error is contributed by fringe count. This, however, is reduced by multiple measurements; and we

estimate the faired line through the mean indices tabulated in Table 1 to be accurate within 0.3%, except in the regions immediately adjacent to an absorption band, where an error as great as 1.0% could occur.

15. RESULTS.

Three runs were made at each selected wave length, and the maximum deviation from the mean of the computed index was three units in the last significant figure. This deviation occurred at 16.00 microns (near the 14.99 micron absorption band), and at 21.50 and 23.00 microns (near the limit of the KBr prism, where signal intensity was low). The deviation in the three computed values for the majority of the experimental points varied from zero to two units in the last significant figure. The indices tabulated in Table 1 are the mean of the three computed values for each point.

Table 1. Refractive Indices of CO_2 at 0° C and 760 mm Hg $(n - 1) \times 10^6$

λ (μ)	Muncie and Whittemore	Wetterblad	Statescu
1.00		450.0	441.4
1.825	584		
2.00		441.1	433.6
2.10	515		
2.17	493		
2.33	466		
2.40		435.1	
2.50	435	431.9	
2.60		428.7	
2.65		427.4	

Table 1. (Continued)

$(n - 1) \times 10^6$

λ (μ)	Muncie and Whittemore	Wetterblad	Statescu
2.67	421		
2.70		429.5	
2.75		431.6	
2.80		432.2	
2.84	424		
2.90	423	426.9	
3.00	417	423.2	418.5
3.30		405.2	
3.36	396		
3.60	373	375.0	
3.80		329.5	
3.90	293	288.0	
4.00	219	217.0	289.0
4.40	753		
4.45		696.0	
4.50		670.7	
4.60	594	617.6	
4.70		584.9	
4.75	552		
4.90	531	548.1	
5.00			531.6
5.02	521		
5.12	509		

Table 1. (Continued)

$(n - 1) \times 10^6$

$\lambda(\mu)$	Muncie and Whittemore	Wetterblad	Statescu
5.20		523.6	
5.27	504		
5.50	493		
5.60		507.0	
6.10	483		
6.20		492.0	
6.70			483.8
6.74	476		
7.00		483.2	
7.10	472		
7.60	471		
8.10	466		
8.55	465		
8.70			458.0
9.00	459	468.2	
9.50	454		
10.00	450	457.7	
10.52	444		
11.00	440	445.5	447.2
11.58	430		
12.00	422		
12.20		423.8	
12.54	404		

Table 1. (Continued)

$(n - 1) \times 10^6$

λ (μ)	Muncie and Whittemore	Wetterblad	Statescu
13.00	383		
13.19			400.4
13.20		371.0	
13.44	347		
13.75		317.0	
14.00	279		
16.00	677		
16.50	635		
17.00	597		
17.50	574		
18.00	560		
18.50	548		
19.00	541		
19.50	536		
20.00	529		
20.50	525		
21.00	523		
21.50	520		
22.00	518		
22.50	516		
23.00	515		
23.50	514		
24.00	511		

16. CONCLUSIONS AND RECOMMENDATIONS.

We have tabulated our results to three significant figures only, on the premise that the fringe count was determined to no greater accuracy than one tenth of a fringe in the majority of the runs. This shortcoming of the system can be overcome by using KBr compensating plates comparable to those of the Jamin Refractometer [5]. With such an installation the accuracy of the fringe count could possibly be increased tenfold, or tc an accuracy of 0.01 fringe.

Radiation intensity can be increased by (1) relocating the Nernst Glower, the "shadow" of which is interposed in the center of the incident radiation due to its location in front of the source mirror; (2) interposing two plane mirrors in the path of the energy between the detector slit and the detector in order to alter the path so that energy from the two center channels that strikes the back of the detector would not be lost; (3) obtaining a new thermocouple of recent design from Charles M. Reeder and Company, which has three times the sensitivity of the one currently in use; (4) obtaining a CsBr prism, which will provide better resolution in the 20-25 micron range, and extend the range of the instrument to 35 microns, if desired.

BIBLIOGRAPHY

1. W. G. Eaton and Frederick H. Thomas, Design and Construction of Instrumentation for Investigating the Optical Dispersion of Gases by Infrared Interferometry, U. S. Naval Postgraduate School, Monterey, California, 1959.

2. Harrison, Lord and Loofbourow, Practical Spectroscopy, Prentice-Hall, Inc., New York, 1949.

3. B. Rossi, Optics, Addison-Wesley Publishing Co., Inc., Reading, Mass., 1957.

4. J. C. Slater and N. H. Frank, Electromagetism, McGraw-Hill Book Co., Inc., New York, 1947.

5. F. A. Jenkins and H. E. White, Fundamentals of Optics, McGraw-Hill Book Co., Inc., New York, 1950.

6. Instruction Manual, Perkin-Elmer Infrared Equipment, Volume 1, The Perkin-Elmer Corp., Norwalk, Conn., 1952.

7. W. E. Williams, Applications of Interferometry, Methuen and Co., Ltd., London, 1950.

8. J. K. Robertson, Introduction to Physical Optics, D. Van Nostrand Co., Inc., New York, 1942.

9. E. L. Quinn and C. L. Jones, Carbon Dioxide, Reinhold Publishing Corp., New York, 1936.

10. International Critical Tables, Vol. VII, Mc Graw-Hill Co., Inc., New York, 1930.

11. Model 13 Ratio Recording Infrared Spectrophotometer Operating and Maintenance Instructions, the Perkin-Elmer Corp., Norwalk, Conn., 1955.

12. Journal of the Optical Society of America, Vol. 43, No. 11, November 1953.

APPENDIX I

Detector Slit Width Determination

The angle between interference principal maxima of a Rayleigh interferometer is given by the expression: [5]

$$d \sin\theta = m\lambda \quad , \quad m = 1$$

for small angles, $\sin\theta = \theta$, so $d\theta = \lambda$, $\theta = \frac{\lambda}{d}$

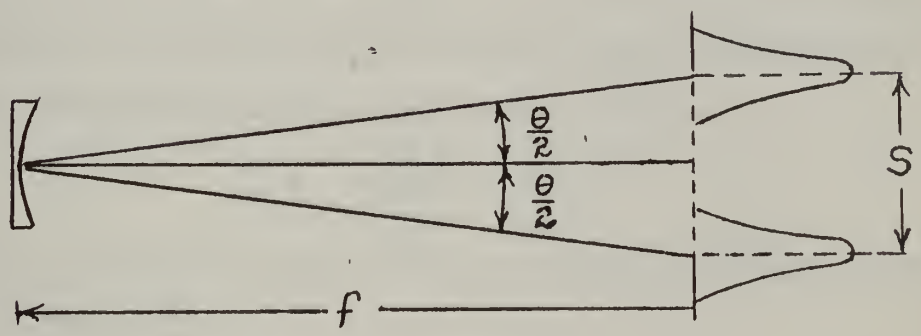

Figure 4. Detector Slit Width Determination

From the geometry of the optical path as seen in Figure 4.

$$\tan\frac{\theta}{2} = \frac{S/2}{f}$$

Again for small angles:

$$\frac{\theta}{2} = \frac{S/2}{f}$$

therefore, for the paraboloidal mirror with a focal length of 267mm., and a slit center to center distance of 5.8 mm.,

$$S = \frac{\lambda f}{d} = \frac{267\lambda}{5.8} = 46\lambda$$

This would provide a slit width which would always have the energy equivalent of one principal maximum present.

For closer analytical control, it would be more desirable to limit the size of the slit so that only one, or part of one particular maximum could possibly be in the slit at any one time. This would lead to

$$S \leq \frac{46\lambda}{2} = 23\lambda$$

or to an angular half width of principal maxima determination as follows: [5]

$$\delta\theta = \frac{\lambda}{A} = \frac{\lambda}{Nd\cos\theta}$$

again for small angles,

$$\frac{\lambda}{6 \times 5.8 \times 1} = \frac{\lambda}{34.8}$$

For a focal length of 267 mm, this results in a linear half width of

$$\frac{2 \times 267}{34.8} = 7.67\lambda$$

Total width of a principal maximum is

$$2 \times 7.67\lambda = 15.34\lambda = \tfrac{1}{3} S$$

Therefore, the optimum detector slit width should be between 15.3 λ and 23 λ . This range positively eliminates the possibility of any out of phase principal maxima appearing in the slit for an infinitely narrow exit slit of the monochromator. The need for a finite exit slit width alters the optimum detector slit width, since allowances must be made for the additional fringe width formed when the exit slit is opened a finite amount. A geometrical determination indicates that combinations of exit and detector slit widths totalling 46 λ will provide singular detection of the desired maxima.

In regions of low radiation intensity, it was found necessary to open the exit slit to 30 λ , in which case the detector slit was set at 16 λ . In a region of relatively high radiation intensity check runs were made with the exit slit opened to the point where the detected fringe was extremely wide due to incident energy of wavelength both shorter and longer than that selected. As expected, absolutely no difference in fringe count was obtained.

APPENDIX II

Determination of Slit Width of the Interferometer

In order to have the individual slits of the interferometer as wide as possible, or a low a/d ratio, but at the same time narrow enough to prevent reflection from the sides of the channels, the following determinations were made:

1. The maximum monochromator exit slit width would be 500 .
2. The length, L, of the monochromator equals 49.52 cm and the focal length of the paraboloidal mirror is equal to 26.7 cm.
3. Width of the channels, D, of the interferometer is 4.78 mm.

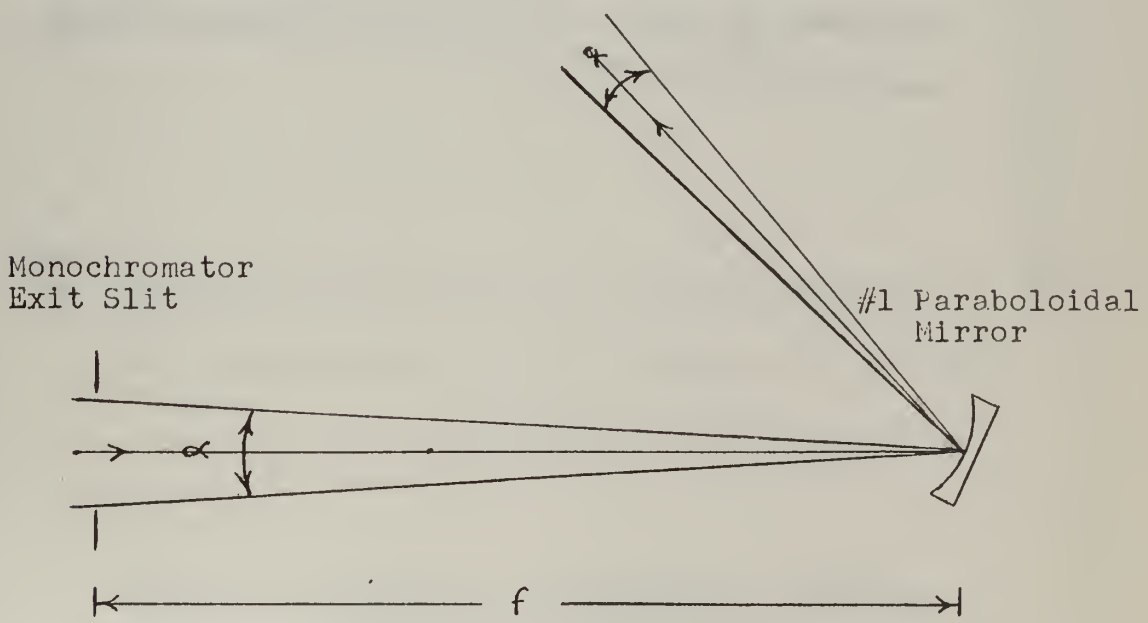

Figure 5. Divergence of Energy due to Exit Slit Width.

To determine optimum value of W:

$$\alpha = \frac{2W}{L} = \frac{g}{f}$$

but L = 49.52 cm and g = 0.5mm., therefore,

$$\frac{2W}{49.52} = \frac{0.5}{26.7}$$

and width of slit of interferometer should be D - 2W or 4.78 - 0.93 = 3.85 mm.

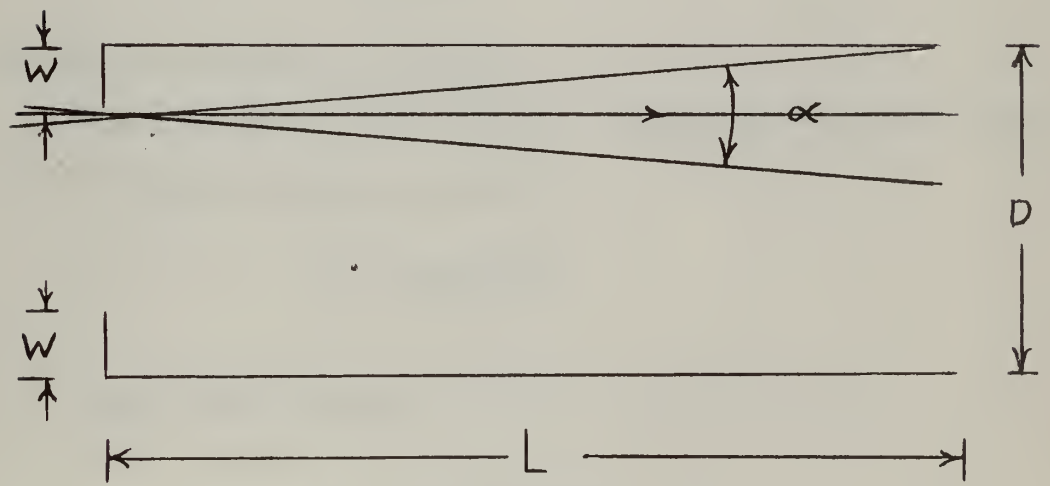

Figure 6. Effect of Divergence of Energy in Interferometer Channel.

APPENDIX III

Determination of Amplitude Magnitude for Alternate Slit System

When the optical path through the vacuum channels of the interferometer and the gas filled channels differs by $m\lambda$, we have the standard six slit interference phenomenon with intensity of the pattern being governed by:

$$I = I_o \frac{\sin^2 \beta}{\beta^2} \frac{\sin^2 N\gamma}{\sin^2 \gamma}$$

For simplification one may deal with amplitude, for which the interference portion of the above expression is:

$$\frac{\sin N\gamma}{\sin \gamma}$$

which is derived as follows:

For two three slit systems (alternate slits of a six slit interferometer), we have:

$$\gamma = \frac{d\pi \sin\theta}{\lambda}$$

Since for alternate slits we have 2d, then

$$2\gamma = \frac{2d\pi \sin\theta}{\lambda}$$

and

$$\frac{\sin 2\gamma}{\sin N2\gamma} = \frac{\frac{1}{2} R_o}{\frac{1}{2} R_1}$$

or

$$R_1 = R_o \frac{\sin N2\gamma}{\sin 2\gamma} \qquad \text{where } N = 3$$

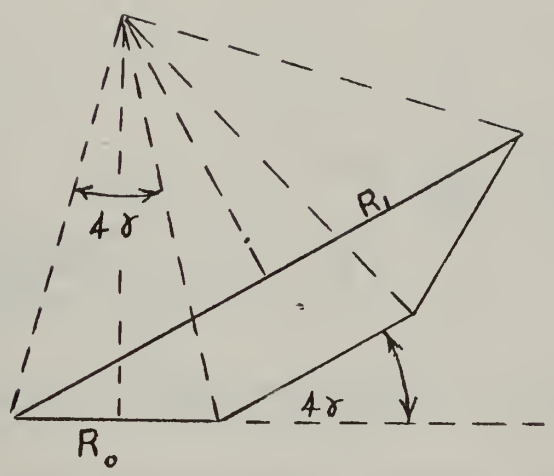

Figure 7. Phase Relationships of Three Alternate Slits

The second set of three slits will be at an angle of 2γ from the first set, so we have:

$$2R_1 \cos\gamma = R$$

Substituting for R_1, we have:

$$2R_o \frac{\sin N2\gamma}{\sin 2\gamma} \cos\gamma = R$$

Letting R_2 represent the resultant of the alternate channels filled by gas, we have:

$$R = 2 R_0 \frac{\sin N2\gamma}{\sin 2\gamma} \cos \frac{2\gamma + \phi}{2}$$

where ϕ is the phase difference of R_2 caused by the gas.

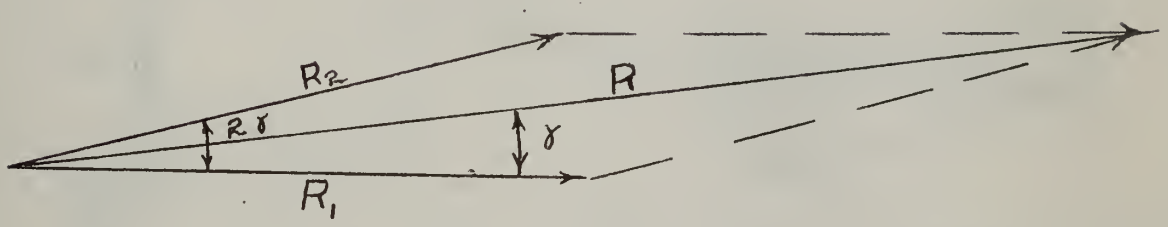

Figure 8. Phase Relationship of Alternate Groups of Three Slits

For a phase difference of ϕ equal to zero, and a trigonometric substitution of

$$\sin 2\gamma = 2 \sin\gamma \cos\gamma$$

we have:

$$R = R_0 \frac{\sin 6\gamma}{\sin\gamma}$$

which is the basic formula for a six slit interference pattern.

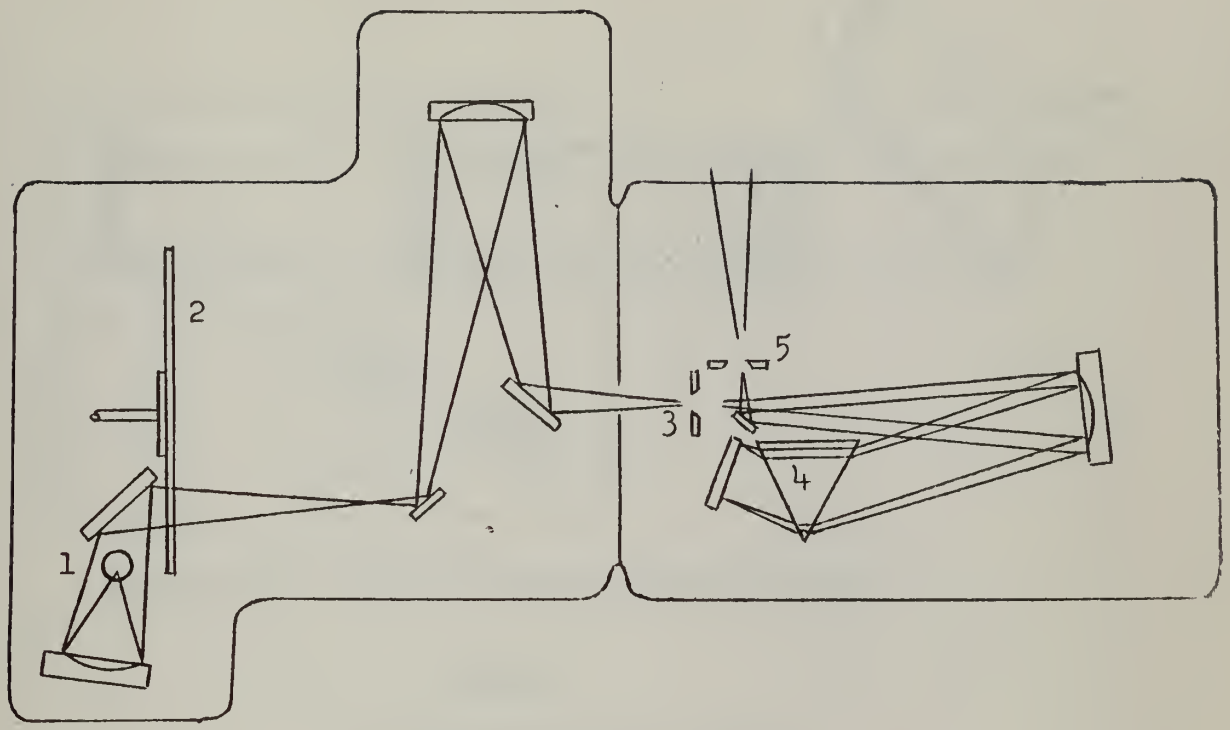

Figure 9. Infrared Source and Monochromator

Legend

1. Infrared Source (Nernst Glower)
2. Chopper
3. Entrance Slit
4. KBr/NaCl Prism
5. Exit Slit

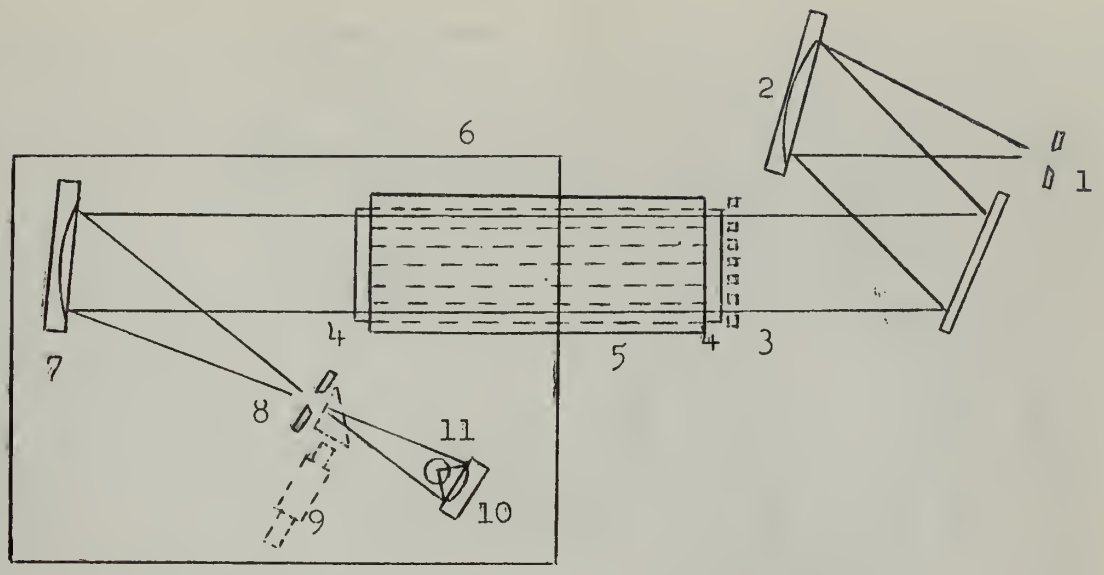

Figure 10. Interferometer Optical System

Legend

1. Monochromator Exit Slit
2. Off-axis Paraboloidal Collimating Mirror
3. Mask, Six Slits
4. KBr Windows
5. Modified Rayleigh Interferometer
6. Light Cover (Not used for our investigation)
7. Off-axis Paraboloidal Collimating Mirror
8. Detector Slit
9. Prism and Microscope (For alignment)
10. Ellipsoidal Mirror
11. Detector

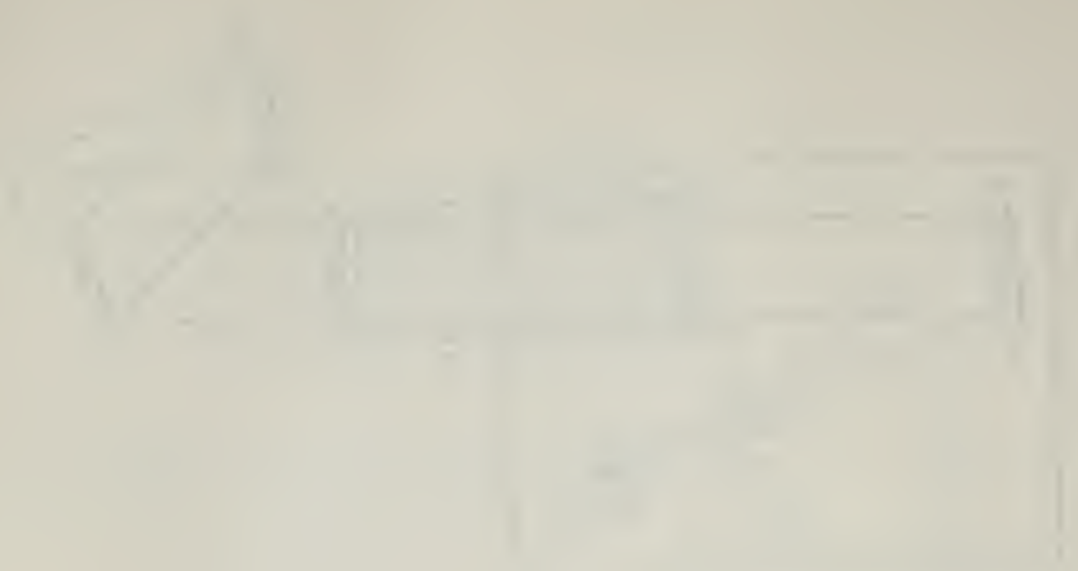

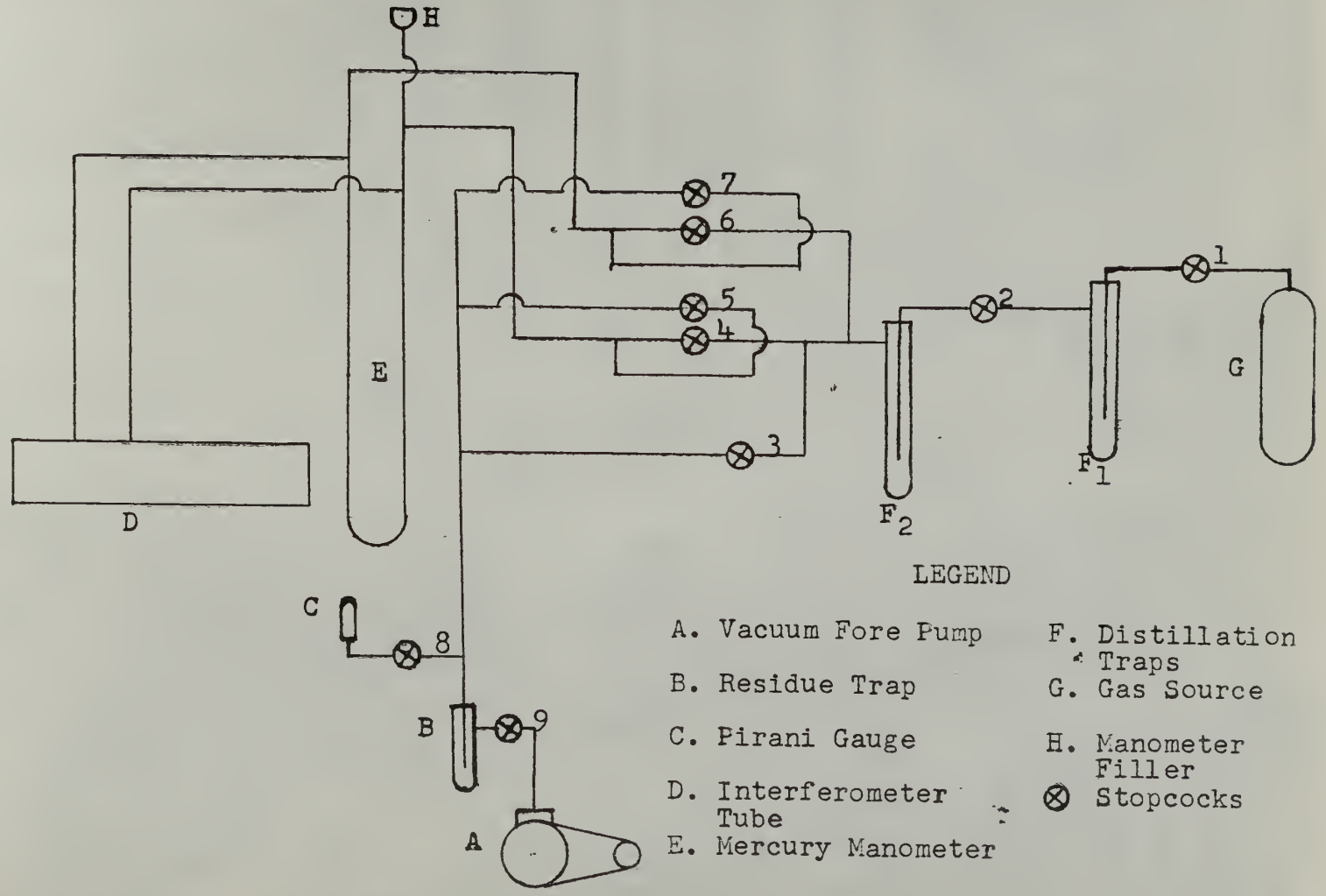

Figure 11. Vacuum and Distillation Systems

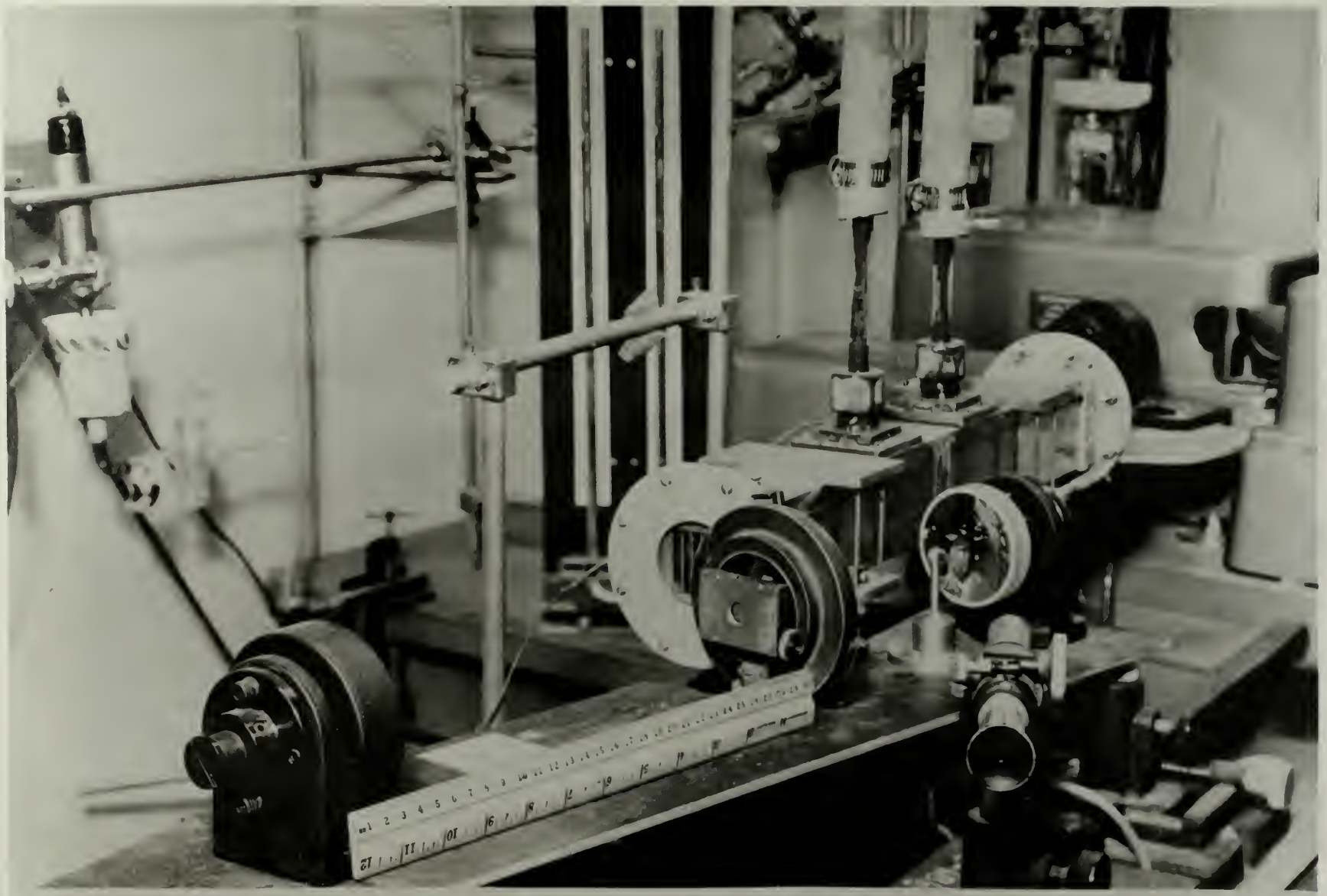

Figure 18. Interferometer and Associated Optical Components

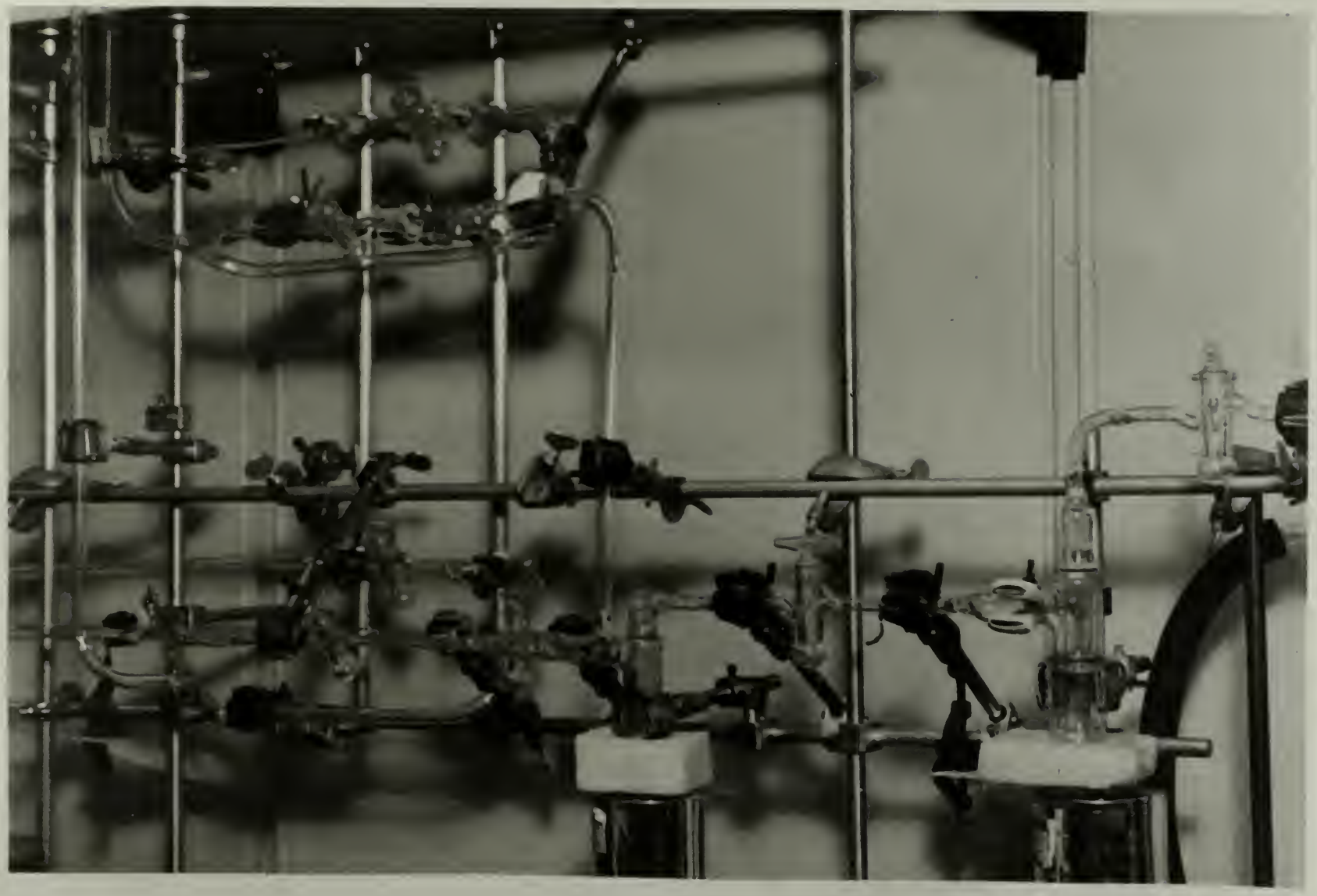

Figure 13. . Vacuum and Gas Adsorption System.

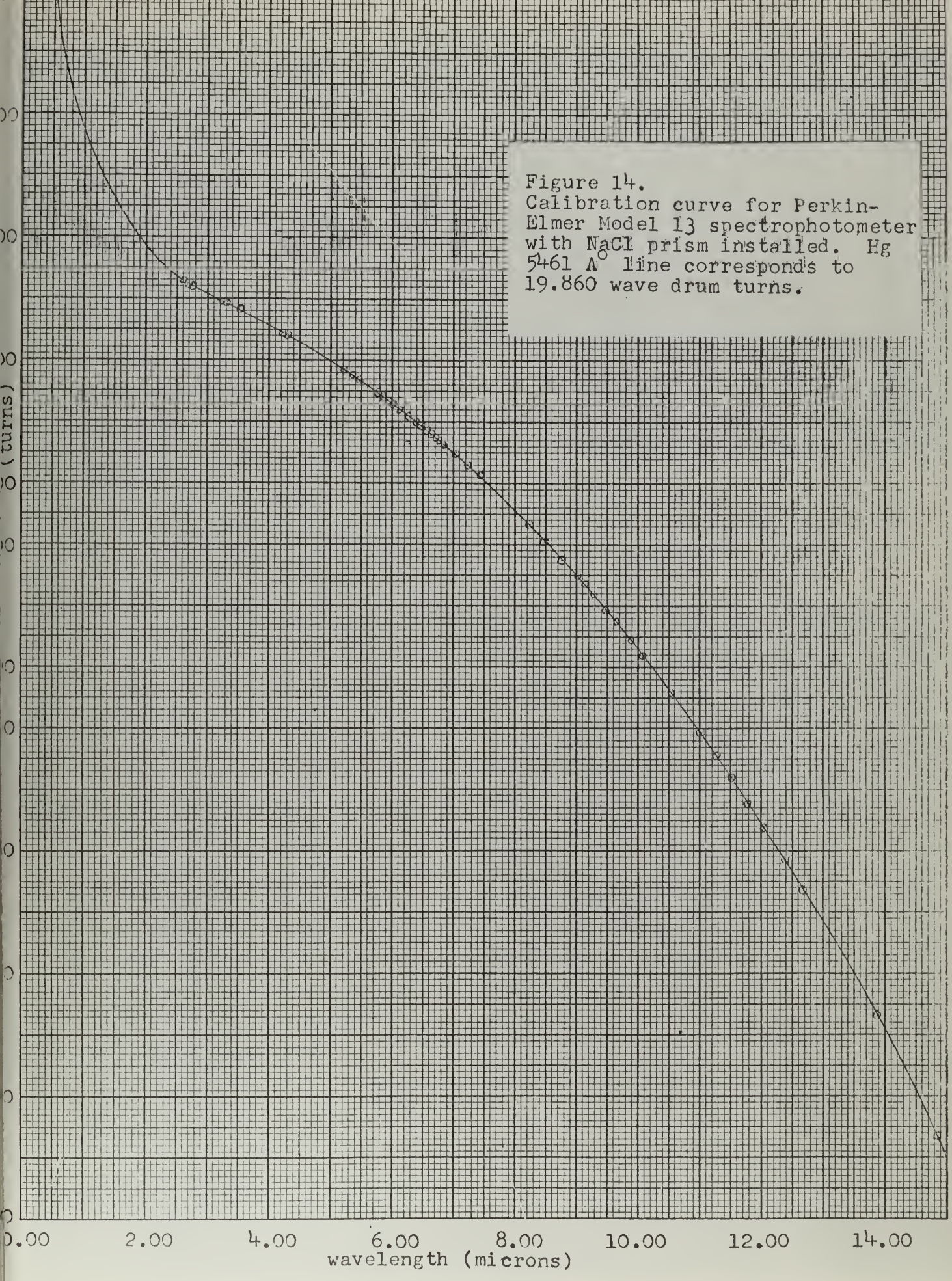

Figure 14.
Calibration curve for Perkin-Elmer Model 13 spectrophotometer with NaCl prism installed. Hg 5461 Å line corresponds to 19.860 wave drum turns.

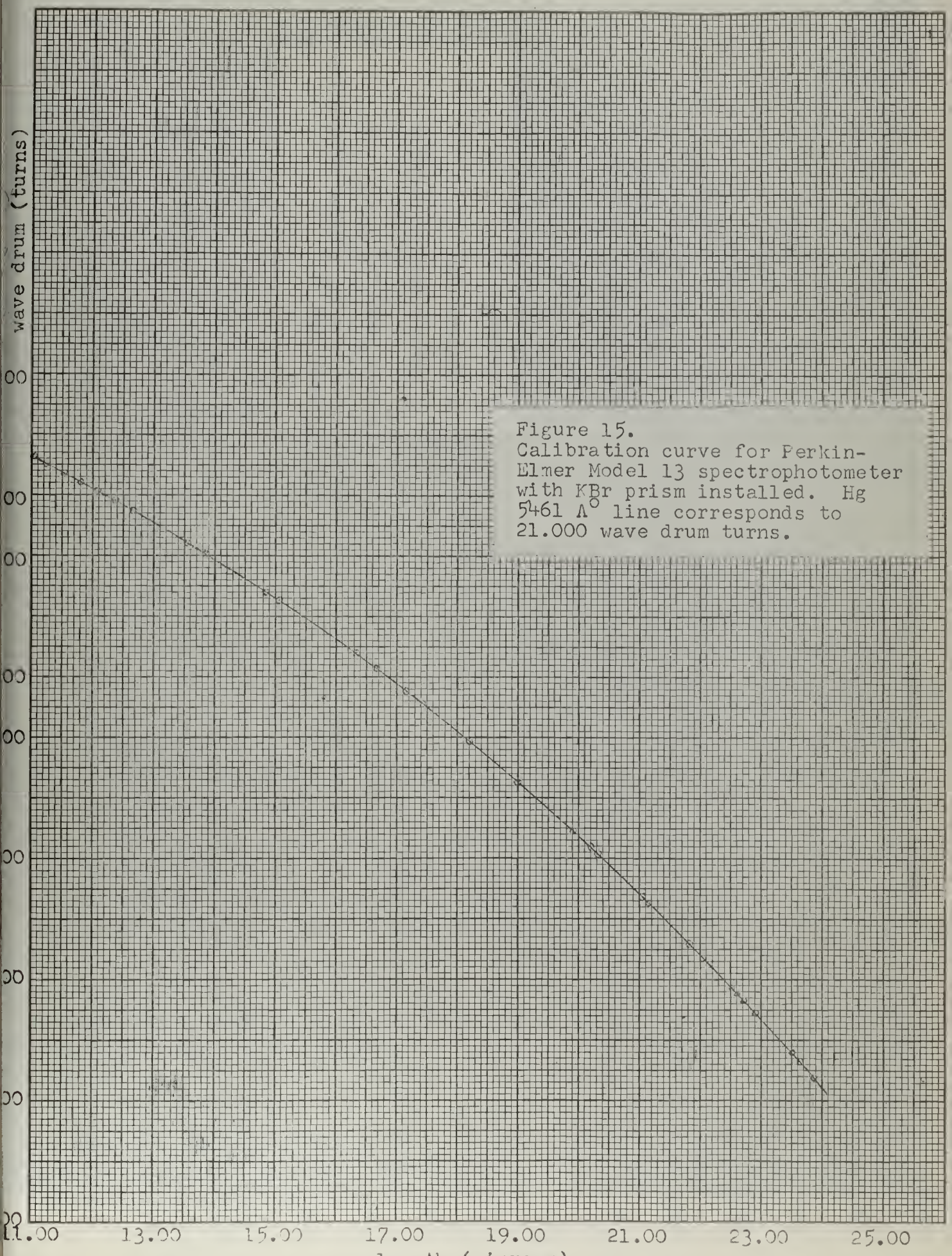

Figure 15.
Calibration curve for Perkin-Elmer Model 13 spectrophotometer with KBr prism installed. Hg 5461 A° line corresponds to 21.000 wave drum turns.

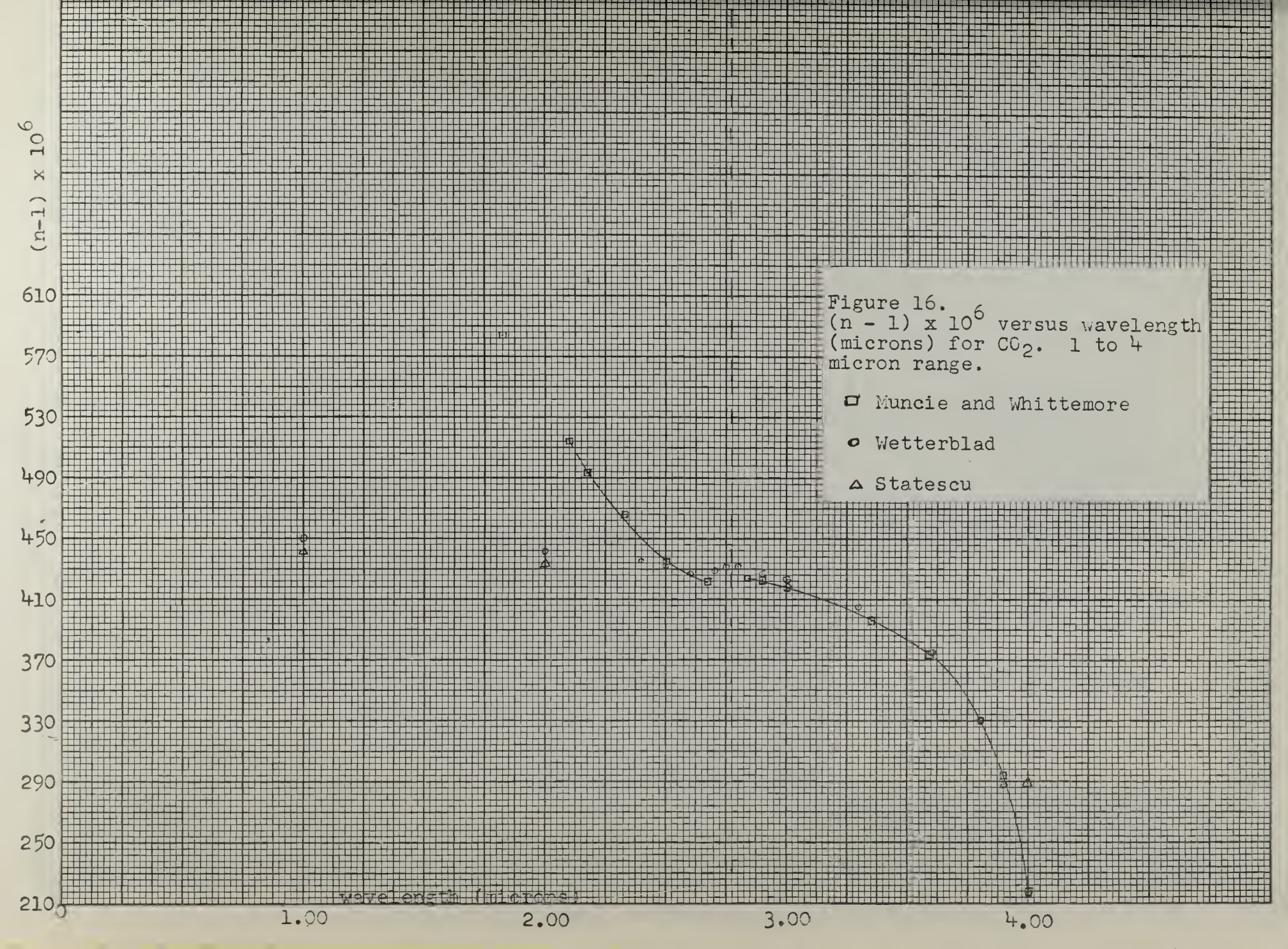

Figure 16.
$(n - 1) \times 10^6$ versus wavelength (microns) for CO_2. 1 to 4 micron range.

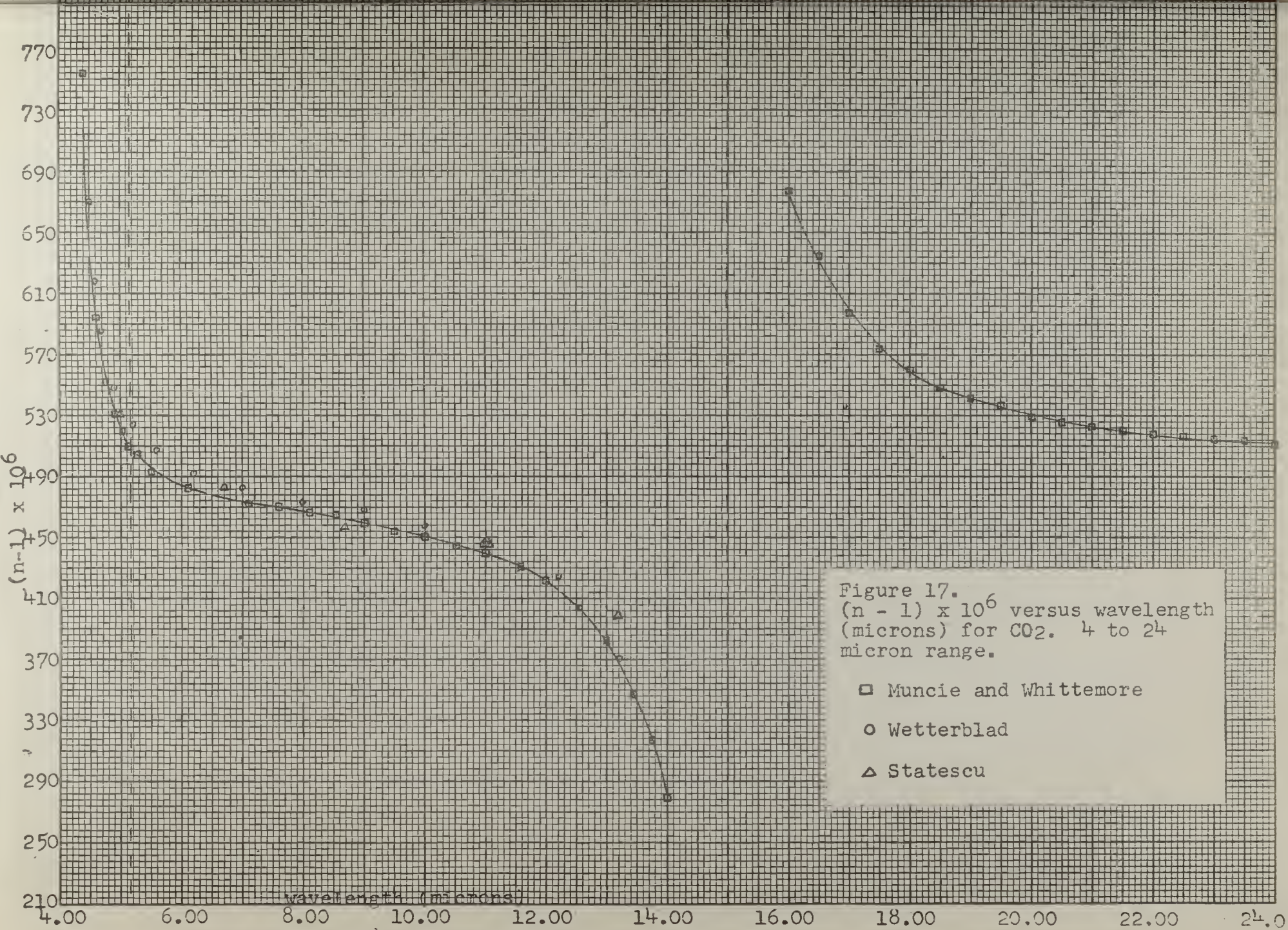

Figure 17.
$(n - 1) \times 10^6$ versus wavelength (microns) for CO_2. 4 to 24 micron range.

□ Muncie and Whittemore

○ Wetterblad

△ Statescu